Stochastic initiation and termination of calcium-mediated triggered activity in cardiac myocytes

Zhen Song[a,b,c,d], Zhilin Qu[a,b,1], and Alain Karma[c,d,1]

[a]Department of Medicine, David Geffen School of Medicine, University of California, Los Angeles, CA 90095; [b]Cardiovascular Research Laboratories, David Geffen School of Medicine, University of California, Los Angeles, CA 90095; [c]Department of Physics, Northeastern University, Boston, MA 02115; and [d]Center for Interdisciplinary Research on Complex Systems, Northeastern University, Boston, MA 02115

Cardiac myocytes normally initiate action potentials in response to a current stimulus that depolarizes the membrane above an excitation threshold. Aberrant excitation can also occur due to spontaneous calcium (Ca^{2+}) release (SCR) from intracellular stores after the end of a preceding action potential. SCR drives the Na^+/Ca^{2+} exchange current inducing a "delayed afterdepolarization" that can in turn trigger an action potential if the excitation threshold is reached. This "triggered activity" is known to cause arrhythmias, but how it is initiated and terminated is not understood. Using computer simulations of a ventricular myocyte model, we show that initiation and termination are inherently random events. We determine the probability of those events from statistical measurements of the number of beats before initiation and before termination, respectively, which follow geometric distributions. Moreover, we elucidate the origin of randomness by a statistical analysis of SCR events, which do not follow a Poisson process observed in other eukaryotic cells. Due to synchronization of Ca^{2+} releases during the action potential upstroke, waiting times of SCR events after the upstroke are narrowly distributed, whereas SCR amplitudes follow a broad normal distribution with a width determined by fluctuations in the number of independent Ca^{2+} wave foci. This distribution enables us to compute the probabilities of initiation and termination of bursts of triggered activity that are maintained by a positive feedback between the action potential upstroke and SCR. Our results establish a theoretical framework for interpreting complex and varied manifestations of triggered activity relevant to cardiac arrhythmias.

calcium wave | delayed afterdepolarization | triggered activity | bistability | arrhythmias

Ventricular arrhythmias, the leading cause of sudden death (1), tend to occur unexpectedly. Understanding their initiation mechanisms remains a major challenge for clinical cardiologists (2). Lethal arrhythmias can occur without any abnormal sign in the ECG, or can be preceded by multiple premature ventricular complexes (PVCs) or short runs of ventricular tachycardia (3). There are many possible sources of randomness that can be responsible for the seemingly unpredictable nature of arrhythmias, such as environmental stresses via neural or metabolic regulations, chaotic dynamics (4, 5), or fluctuations associated with the intrinsic stochasticity of ion channel kinetics (6, 7).

During normal contraction, calcium (Ca^{2+}) release from the sarcoplasmic reticulum (SR)—the intracellular Ca^{2+} store of a ventricular myocyte—is triggered by Ca^{2+} entry into the cell via L-type calcium channels (LCCs), a mechanism known as Ca^{2+}-induced Ca^{2+}-release (CICR). However, SR Ca^{2+} release can also occur spontaneously, as observed in a variety of pathological conditions ranging from heart failure (8, 9) to ischemia (10) to catecholaminergic polymorphic ventricular tachycardia (11–14). Spontaneous Ca^{2+} release (SCR) transiently elevates the cytosolic Ca^{2+} concentration ($[Ca]_i$), which in turn increases the forward mode of the electrogenic Na^+/Ca^{2+} exchange (NCX) current (I_{NCX}). In this mode, NCX brings into the cell three Na^+ for each Ca^{2+} it extrudes, thereby depolarizing the membrane. In the common situation where SCR occurs after a delay following the

end of an action potential (AP), it induces a so-called "delayed afterdepolarization" (DAD). When, furthermore, the DAD is of sufficient amplitude for the transmembrane voltage (V_m) to exceed the threshold for activation of the Na^+ current (I_{Na}), this "suprathreshold" DAD causes a triggered action potential (TAP). In contrast, a "subthreshold" DAD only causes a small transient elevation of V_m. Triggered activity (TA) refers to the generation of a TAP and must be preceded by at least one stimulated AP that acts as the "trigger." This distinguishes TA from "automaticity," which refers to the ability of a cell to depolarize itself and generate an AP without a trigger.

The physiological conditions that promote Ca^{2+}-mediated TA are qualitatively understood (15–17). The Ca^{2+} release channels, called ryanodine receptors (RyRs), typically need to have increased sensitivity to cytosolic Ca^{2+} so as to facilitate RyR openings and Ca^{2+} release. Additionally, the SR Ca^{2+} concentration (SR load) needs to be sufficiently high to sustain a high Ca^{2+} release flux. Both fast pacing and β-adrenergic stimulation, which potentiates both LCC and the SR Ca^{2+}-ATPase (SERCA), tend to increase SR load. Increased SR load together with RyR hyperactivity can then jointly promote the initiation and propagation of intracellular Ca^{2+} waves that are the hallmark of SCR (18, 19).

Beyond this pictorial level, TA remains poorly understood. TA seems to occur randomly, but with largely unknown statistical properties. It can be manifested as a single TAP, a burst of several TAPs, or even focal activity in the form of sustained V_m oscillations

(14, 20–33). How deterministic and stochastic dynamics cooperate to cause those behaviors and transitions between them is unclear.

Randomness of TA in ventricular myocytes would be naively expected to stem from the stochastic nature of SCR at the whole-cell level. RyR channels are known to form clusters of 50–200 RyRs colocalized with a few LCCs at Ca^{2+} release units (CRUs). Approximately 20,000–50,000 CRUs are spatially organized in a 3D array inside a myocyte (34–36). Stochastic opening of a large enough number of RyRs in a CRU can trigger firing of a local spike of $[Ca]_i$, which then diffuses to induce RyR openings in neighboring CRUs. It enables one or more Ca^{2+} waves to propagate throughout the cell by this fire–diffuse–fire process, causing a global (whole-cell) spike of $[Ca]_i$. Statistical properties of those global spikes have been extensively studied (28, 37) in eukaryotic cells where clusters of inositol trisphosphate receptors (Ca^{2+} release channels) have an analogous role to RyR clusters in cardiac myocytes. Spiking is typically random in those cells. However, statistical properties of SCR remain largely unexplored in the more complex setting of cardiac myocytes where the Ca^{2+} dynamical subsystem, consisting of Ca^{2+} release and uptake, is tightly bidirectionally coupled to V_m dynamics. In one direction ($V_m \rightarrow [Ca]_i$), the AP upstroke triggers nearly synchronized Ca^{2+} releases from CRUs by LCC-mediated CICR. In the opposite direction ($[Ca]_i \rightarrow V_m$), the resulting transient rise of $[Ca]_i$, which can also result from SCR, influences V_m dynamics by its effect on Ca^{2+}-sensitive membrane currents (primarily the L-type Ca^{2+} current, $I_{Ca,L}$, and the NCX current, I_{NCX}). Because V_m diffusion is several orders of magnitude faster than Ca^{2+} diffusion, V_m is spatially uniform on the scale of a myocyte. Consequently, stochastic effects of individual membrane ion channel openings are spatially averaged out on that scale and, with rare exceptions (6, 7), the whole-cell V_m dynamical subsystem generically exhibits deterministic dynamics. V_m dynamics can potentially become more random in conditions where Ca^{2+} waves are present, and SCR generates global spikes of $[Ca]_i$ causing DADs. It is well appreciated that the coupling of Ca^{2+} cycling and excitation can potentiate arrhythmias (4, 38–42). However, how TA emerges from the interplay of a nearly deterministic V_m subsystem and a highly stochastic Ca^{2+} cycling subsystem remains largely unknown.

In this study, we use computer simulations of a physiologically detailed ventricular myocyte model (43, 44) to investigate the statistical and dynamical properties of TA. This multiscale model bridges the submicron scale of individual CRUs and the whole cell, and uses Markov models to treat fully stochastically the kinetics of both LCCs and RyRs colocated at each CRU. Hence, this model captures both the stochastic spatially distributed nature of Ca^{2+} release, including Ca^{2+}-wave mediated SCR, and the bidirectional coupling of Ca^{2+} and V_m dynamics, with membrane ionic currents taken from a well-established rabbit ventricular AP model (45).

Our results demonstrate that both the initiation and termination of TA are random processes controlled by large fluctuations of whole-cell Ca^{2+} concentration spike amplitude (peak $[Ca]_i$) resulting from SCR, but not spike timing as in other eukaryotic cells such as *Xenopus* oocytes (46–49) where Ca^{2+} dynamics is not coupled to V_m. In cardiac myocytes, the AP upstroke triggers nearly synchronized Ca^{2+} release, causing RyRs to recover and hence SCR to occur at a relatively precise time interval after this upstroke, which follows a narrow distribution. In contrast, the Ca^{2+} spike amplitudes follow a broad normal distribution. We show that the width of this distribution, which underlies randomness in TA, is controlled by fluctuations in the number of Ca^{2+} wave foci. From the knowledge of this distribution, we compute quantitatively the probabilities of initiation and termination of TA and obtain a unified theoretical framework to interpret a wealth of different dynamical behaviors. With increasing degree of instability of the Ca^{2+} subsystem (increasing RyR leakiness and SR Ca^{2+} load), those behaviors range from normal excitation–contraction coupling, with Ca^{2+}

dynamics slaved to V_m, to burst-like TA. Bursting is further shown to result from bistability between the stable resting state and a metastable limit cycle, consisting of coupled $[Ca]_i$ and V_m oscillations promoted by a positive feedback between SCR and AP upstroke.

Results

Stochastic Initiation and Termination of TA During Sustained and Interrupted Pacing. DADs and TA are induced in the cell model by mimicking the combined effects of β-adrenergic stimulation and increased RyR channel activity. This combination is traditionally used to induce DADs and TA (12, 14, 18, 19). β-Adrenergic stimulation is modeled by increasing $I_{Ca,L}$ and SERCA activity, mimicking the effect of isoproterenol (ISO) addition (*Methods*). RyR hyperactivity is modeled by multiplying the individual RyR channel closed to open rate by a multiplicative factor α. Increasing α shifts the EC_{50} of the dose–response curve of RyR open probability to lower $[Ca]_i$ and has an effect similar to caffeine addition (19). The dynamics of TA is studied as a function of both α and the pacing cycle length (PCL).

Fig. 1A summarizes the observed AP dynamics. In the green zone where either α is small or PCL is long, only subthreshold DADs, whose amplitudes are not large enough to induce TA, occur between pacing beats (Fig. 1B). When α is increased or the PCL is decreased, suprathreshold DAD-induced TA occurs in the blue zone (example in Fig. 1C). When the PCL is further decreased to fall inside the red zone in Fig. 1A, the next AP upstroke occurs before a subthreshold or suprathreshold DAD could form, and thus no DADs or TA can be observed between stimulate APs. After the pacing stops, DADs or TA can then be observed (example in Fig. 1D). This is the typical pacing protocol used in experiments to induce DADs and TA. In both pacing protocols (blue and red zones), TA is observed to be either transient for RyR hyperactivity less than some threshold $\alpha < 3.3$ or sustained for $\alpha \geq 3.3$ (example in Fig. 1E), corresponding to the regions left and right of the dashed line in Fig. 1A, respectively.

The Number of Beats Before Initiation and Before Termination of TA Follow Geometric Distributions. Due to the random variation of the DAD amplitude, the number of DADs (N_{DAD}) preceding TA is random. The duration of the TA burst measured by the number of TAPs (N_{TAP}) is also random. We investigate the statistical properties of both the random initiation of TA (see *SI Appendix*, Fig. S1, for sample traces) during sustained pacing and the random termination of TA (see *SI Appendix*, Fig. S2, for sample traces) induced after a pacing pause. For this purpose, we perform at least 500 random trials for each parameter set of interest.

For initiation of TA, we record the number of paced beats yielding only subthreshold DADs (N_{DAD}) before a suprathreshold DAD that produces a TAP. A histogram of N_{DAD} illustrated in Fig. 2A exhibits a broad distribution. Semilog plots of normalized event probability (Fig. 2B) show that the distribution is geometric. N_{DAD} depends on the degree α of RyR hyperactivity and increasing α decreases the average N_{DAD}. The initiation of TA also depends on PCL because the SR load generally increases with decreasing PCL. Fig. 2C shows N_{DAD} histograms for different PCLs. As the pacing becomes faster, the number of DADs before TA initiation is smaller.

For termination of TA, we record the number of triggered beats, that is, the number of TAPs (N_{TAP}) in a TA burst occurring before the membrane voltage returns to the resting state and construct similar histograms. The N_{TAP} histograms also exhibit geometric distributions (Fig. 2 D–F), which also depend on α. The average value of N_{TAP} increases as α increases (Fig. 2E). However, unlike N_{DAD}, N_{TAP} does not depend on PCL (Fig. 2F). As we shall see later, this property stems from the fact that termination of TA corresponds to the escape from a limit cycle
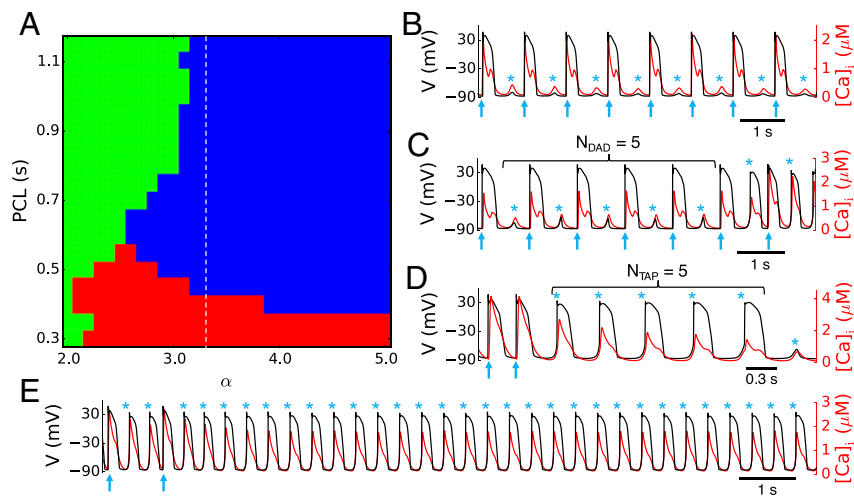
Fig. 1. Stochastic initiation and termination of triggered activity (TA). (*A*) Excitation pattern diagram distinguishing different dynamical behaviors as a function of pacing cycle length (PCL) and RyR Ca^{2+} release channel hyperactivity where increasing α beyond the control value $\alpha = 1$ increases RyR open probability: only subthreshold DADs and no TA (green), suprathreshold DADs initiating TA between paced beats (blue), and TA after pacing is stopped (red). TA is transient and sustained to the left and right of the dashed line corresponding to $\alpha = 3.3$, respectively. (*B–E*) Illustrative transmembrane voltage (black) and cytosolic Ca^{2+} concentration $[Ca]_i$ (red) traces for the different colored regions: $\alpha = 2.5$ and PCL = 1 s (*B*); $\alpha = 3.3$ and PCL = 1 s (*C*); $\alpha = 3.1$ and PCL = 0.3 s (*D*); $\alpha = 4.5$ and PCL = 1 s (*E*). Arrows indicate paced beats and stars (*) indicate subthreshold DADs or TA.

that is sustained by a positive feedback between SCR and AP excitation and that is independent of pacing history.

It should be noted that N_{DAD} and N_{TAP} follow geometric distributions only after a certain number of beats (Fig. 2). This is because, depending on the protocol used to induce TA, it takes one to a few beats for the Ca^{2+} cycling dynamics to relax to a new steady state after a sudden β-adrenergic stimulation (ISO addition) or cessation of pacing. For the same reason, N_{TAP} distributions for smaller α values (*SI Appendix*, Fig. S3) are very different from geometric distributions because TA terminates before Ca^{2+} cycling has relaxed to the steady state after pacing is stopped.

The timing of SCR events is much less random than the peak $[Ca]_i$. To characterize this randomness, we measure the latency of SCR defined as the time interval between the previous AP upstroke and the time at which the next DAD/TAP reaches its peak. The results show that the distributions are comparatively much narrower (see *SI Appendix*, Fig. S4, for details).

The Amplitudes of SCRs Underlying DADs Follow a Broad Normal Distribution. Ca^{2+}-mediated TA traditionally occurs when the peak value of the whole-cell $[Ca]_i$ following a SCR is large enough to drive enough I_{NCX} to depolarize the membrane above the I_{Na} activation threshold for eliciting an AP. To characterize the mechanism underlying the randomness in initiation and termination of TA, we therefore study the statistic properties of peak $[Ca]_i$ under different conditions. Fig. 3*A* shows the histogram of peak $[Ca]_i$ for a case with no TA (the case in Fig. 1*B*). The distribution is well approximated by a normal (Gaussian)
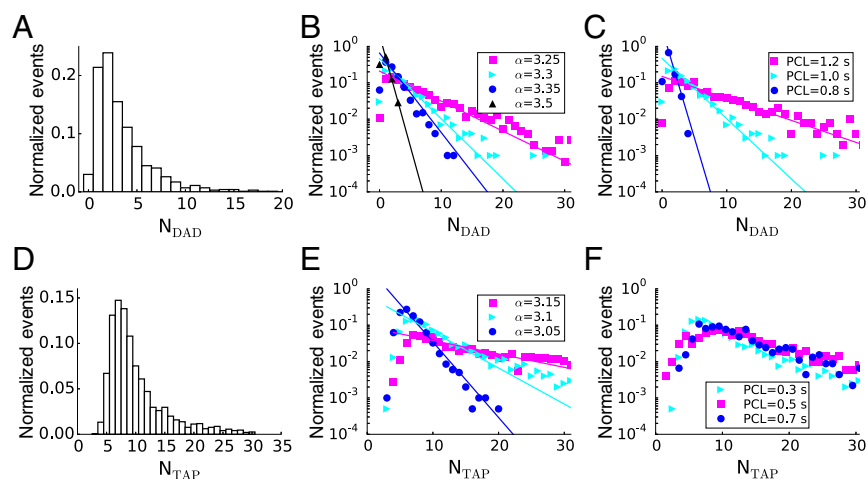

Fig. 2. Statistical properties of stochastic initiation and termination of TA. (*A*) Histogram of N_{DAD} for a total of 1,000 trials, PCL = 1 s, and $\alpha = 3.3$. (*B*) N_{DAD} distributions in semilog plot for four different α values, PCL = 1 s. Lines are best fits to Eq. **1** for the decreasing part of the N_{DAD} distributions. R^2 values of the best fits for the four α values are 0.992 ($\alpha = 3.25$), 0.998 ($\alpha = 3.3$), 0.984 ($\alpha = 3.35$), and 0.999 ($\alpha = 3.5$). (*C*) N_{DAD} distributions in semilog plot for three PCL values ($\alpha = 3.3$). Lines are best fits to Eq. **1** for the decreasing part of the N_{DAD} distributions. R^2 values of the best fits for the three PCL values are 0.999 (PCL = 0.8 s), 0.998 (PCL= 1 s), and 0.957 (PCL = 1.2 s). (*D*) Histogram of N_{TAP} for a total of 2,000 trials, PCL = 0.3 s, and $\alpha = 3.1$. (*E*) N_{TAP} distributions in semilog plot for three different α values, PCL = 0.3 s. Lines are best to Eq. **3** of the N_{TAP} distribution. R^2 values of the best fits for the three α values are 0.994 ($\alpha = 3.05$), 0.985 ($\alpha = 3.1$), and 0.888 ($\alpha = 3.15$). (*F*) N_{TAP} distributions in semilog plot for three different PCLs ($\alpha = 3.1$).
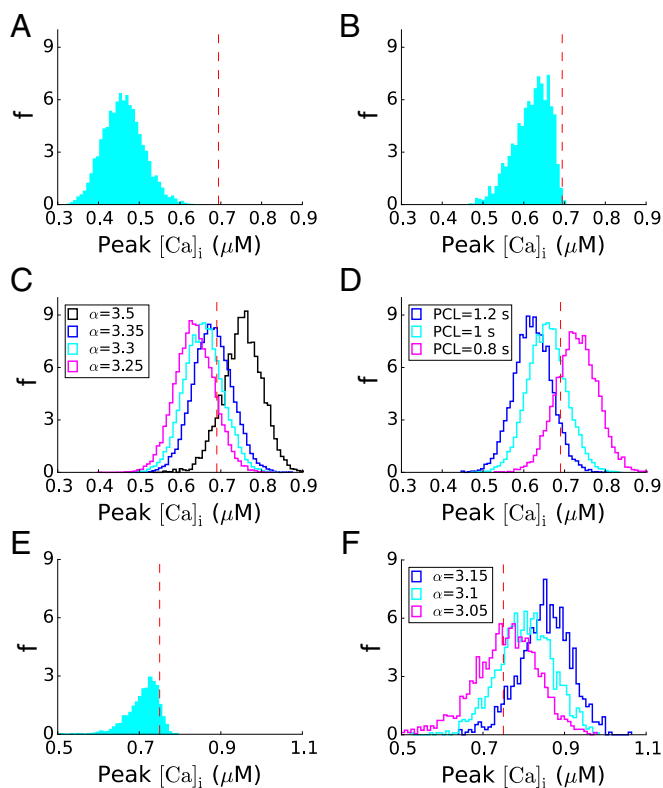
Fig. 3. Distributions of spontaneous Ca^{2+} release (SCR) amplitude. (*A*) SCR amplitude (peak [Ca]$_i$) distribution for PCL = 1 s and α = 2.5 (corresponding to Fig. 1*B*). (*B*) SCR amplitude distribution for PCL = 1 s and α = 3.3 (corresponding to Fig. 1*C*). (*C*) SCR amplitude distribution for four α values (corresponding to Fig. 2*B*; PCL = 1 s) under the condition in which I_{Na} and $I_{Ca,L}$ are blocked during diastolic intervals. Block prevents TA initiation and allows us to characterize the distributions over the entire range of SCR amplitude. (*D*) SCR amplitude distribution for three PCLs (corresponding to Fig. 2*C*) in which I_{Na} and $I_{Ca,L}$ are blocked during diastolic intervals. (*E*) SCR amplitude distribution for the subthreshold DAD at termination of TA (α = 3.1 and PCL = 0.3 s). (*F*) SCR amplitude distribution obtained using the 11th SCR during which I_{Na} and $I_{Ca,L}$ are blocked for three different α values (PCL = 0.3 s). The dashed vertical lines denote the [Ca]$_i$ thresholds (Ca$_{th}$ in Eqs. 2 and 4) for TA initiation in *A–D* and TA termination in *E* and *F*.

distribution. Fig. 3*B* shows the histogram of peak [Ca]$_i$ for the case corresponding to Fig. 1*C* where TA occurs. In this case, the distribution is truncated at a [Ca]$_i$ threshold (Ca$_{th}$) of ~0.69 μM, corresponding to the dashed lines in Fig. 3 *A–D*. Peak [Ca]$_i$ values larger than this threshold produced a suprathreshold DAD that initiates TA. Hence, Ca$_{th}$ represents the [Ca]$_i$ spike amplitude threshold for TA. To obtain a complete and steady-state distribution of the peak [Ca]$_i$, we block both I_{Na} and $I_{Ca,L}$ during the diastolic phases so that no TA is elicited when [Ca]$_i$ is above Ca$_{th}$. In addition, instead of many trials, a single long simulation, which is equivalent in this case to several independent simulations, is carried out to obtain the peak [Ca]$_i$ distribution. Fig. 3*C* shows the peak [Ca]$_i$ distributions for four α values, which all follow normal distributions. Increasing α strengthens SCR and thus right shifts the peak [Ca]$_i$ distribution to higher [Ca]$_i$. Increasing the pacing rate also right shifts the distribution (Fig. 3*D*) because faster pacing increases SR load and produces larger amplitude SCRs.

Similarly, we measure the peak [Ca]$_i$ distribution for the DAD right after the termination of TA by repeating the simulations many times (>2,000 times). Because TA is terminated by a subthreshold DAD (e.g., the DAD after the burst of five TAPs in Fig. 1*D*), the distribution of peak [Ca]$_i$ in this case is truncated, as indicated by the dashed line in Fig. 3*E*. To measure the full

distribution composed of the subthreshold DADs that terminate TA and the suprathreshold DADs that sustain TA, we blocked I_{Na} and $I_{Ca,L}$ after the 10th AP of a TA burst and measured the peak [Ca]$_i$ of the 11th SCR. By repeating this simulation many times (>1,500 times), we obtained the peak [Ca]$_i$ distribution underlying both subthreshold and suprathreshold DADs (Fig. 3*F*), which is also well approximated by a normal distribution.

Linking Quantitatively the Normal Distributions of SCR Amplitude and the Geometric Distributions of the Number of Beats Before or After Initiation of TA. Based on the finding that the amplitude of SCRs (peak [Ca]$_i$) closely follows a normal distribution (Fig. 3), one can assume that SCRs are independent random events, with the amplitude of SCR drawn at each beat from this distribution. It follows naturally from this assumption that N_{DAD} follows a geometric distribution:

$$F_{DAD}(N_{DAD}) = (1 - p_{DAD})(p_{DAD})^{N_{DAD}}, \qquad [1]$$

where

$$p_{DAD} = \int_0^{Ca_{th}} f(Ca)\,dCa \qquad [2]$$

is the probability of observing a subthreshold SCR and $(1 - p_{DAD})$ is the probability of observing a suprathreshold SCR, where $f(Ca)$ is the probability density function of the peak [Ca]$_i$ distribution. Given these definitions, Eq. 1 is simply the probability of observing N_{DAD} subthreshold DADs followed by one suprathreshold DAD initiating TA. Next, we best fit the decreasing part of the N_{DAD} distributions in Fig. 2 *B* and *C* to Eq. 1 and plot the corresponding best fits as lines in Fig. 2 *B* and *C*. These best fits are used to obtain p_{DAD} values for different α and PCLs. The convergence of the results as a function of the number of statistical samples is shown in *SI Appendix*, Fig. S5. We then use Eq. 2 together with the obtained p_{DAD} values and Gaussian fits of the [Ca]$_i$ peak distributions in Fig. 3 *C* and *D* to obtain the Ca$_{th}$ values. The results reported in *SI Appendix*, Tables S1 and S2, show that the Ca$_{th}$ values are very close to the threshold (~0.69 μM) deduced from the truncated peak [Ca]$_i$ distribution in Fig. 3*B*. This indicates that the theoretical prediction of Eq. 1 agrees well with the simulation results, thereby validating quantitatively our assumption that SCRs following each paced beat are independent random events for large enough N_{DAD}.

Similarly, the number of suprathreshold DADs before a subthreshold DAD that terminates TA also follows a geometric distribution:

$$F_{TAP}(N_{TAP}) = (1 - p_{TAP})(p_{TAP})^{N_{TAP}}, \qquad [3]$$

where

$$p_{TAP} = \int_{Ca_{th}}^{\infty} f(Ca)\,dCa \qquad [4]$$

is the probability of observing a suprathreshold SCR and $(1 - p_{TAP})$ is the probability of observing a subthreshold SCR that terminates the burst. Following the same method as for N_{DAD} distributions, we best fit the decreasing part of the N_{TAP} distributions shown in Fig. 2*E* to Eq. 3. The best fits corresponding to the lines in Fig. 2*E* are used to obtain p_{TAP} values. We then use Eq. 4 together with the obtained p_{TAP} values and Gaussian fits to [Ca]$_i$ peak distributions in Fig. 3*F* to obtain the Ca$_{th}$ values. The results reported in *SI Appendix*, Table S3, show that the obtained Ca$_{th}$ values are very close to the threshold (~0.75 μM) deduced from the truncated

peak [Ca]$_i$ distribution in Fig. 3E. This indicates that the theoretical prediction of Eq. **3** (lines in Fig. 2E) agrees well with the simulation results (symbols in Fig. 2E), thereby validating our assumption that SCRs in a long TA burst are independent random events. We note that Ca$_{th}$ differs slightly for initiation and termination of TA (0.69 μM in Fig. 3B vs. 0.75 μM in Fig. 3E; *SI Appendix*, Fig. S6). This difference is explained later in *Discussion*.

Fluctuations in the Number of Independent Ca^{2+} Wave Foci Underlie Randomness in Whole-Cell SCR Amplitudes. Simulations show that each SCR event is the summation of multiple Ca^{2+} waves emanating from different foci randomly distributed throughout the cell (*Movie S1*). By visual analysis of a few movies, we estimate the number of foci N_f to increase between about 20 and 50 with increasing hyperactivity of RyRs. However, the spatially distributed and stochastic nature of SCR makes it generally difficult to automatize the counting of N_f in the detailed model simulations and to gather enough statistics to relate the probability distribution of N_f with the SCR amplitude distribution. To relate those distributions, we construct a simplified model of SCR that captures salient features of Ca^{2+} wave initiation and propagation. Despite its simplicity, this model nontrivially reproduces the normal SCR amplitude distribution observed in the detailed model simulations and shows that this distribution exists over a broad range of N_f values including values <10 typically observed in experiments (14). Variability in SCR amplitude ([Ca]$_i$ peak value) can in principle originate from variability in the number of foci and/or variability in the timing of the foci. Detailed model simulations show that the distribution of the time interval between the [Ca]$_i$ peak and the end of the previous AP is relatively narrow (*SI Appendix*, Fig. S4), suggesting that variability of the number of Ca^{2+} waves is primarily responsible for the variability of SCR amplitude. Accordingly, we base the simplified SCR model on the following three assumptions:

i) Starting from some arbitrary origin of time when RyR channels are fully recovered, Ca^{2+} waves foci are initiated randomly anywhere inside the cell by recruiting a single CRU with a probability k_f per unit time per unit volume (i.e., k_f is spatially uniform).

ii) Once a CRU is recruited, the resulting Ca^{2+} wave propagates deterministically at a constant speed c (by recruiting neighboring CRUs with a delay time equal to a/c, where a is the spacing between CRUs) until it collides with another Ca^{2+} wave or the boundary.

iii) Each CRU recruited by a Ca^{2+} wave causes a local transient increase of [Ca]$_i$ with a fixed spark profile fitted to detailed model simulations (*SI Appendix*, Fig. S7), and the whole-cell [Ca]$_i$ is the summation of all the local [Ca]$_i$ profiles.

The model is taken to have the same number of CRUs as the detailed model and is simulated 10,000 times for different values of k_f to obtain sufficient statistics. Fig. 4A shows the distributions of the number of foci for three different k_f, whereas Fig. 4B shows the corresponding peak [Ca]$_i$ distributions. For a larger k_f, there are more foci and the peak [Ca]$_i$ is higher. Fig. 4C plots the coefficient of variation σ/μ of the peak [Ca]$_i$ distributions (where σ and μ are the standard deviation and mean of the distributions, respectively) vs. the average number of foci $<N_f>$ generated using different k_f. The results show that σ/μ decreases approximately as $1/\sqrt{<N_f>}$, indicating that SCR amplitude fluctuations are controlled primarily by the number of Ca^{2+} wave foci. Of note, Fig. 4D shows that the coefficient of variation for the number of wave foci is $1/\sqrt{<N_f>}$. Fig. 4 E and F plot the peak [Ca]$_i$ distributions and σ/μ ratio from simulations of the detailed model for four different α values, showing that as the RyR becomes more sensitive to Ca^{2+}, the peak [Ca]$_i$ distribution shifts to the right and σ/μ decreases.

The lattice model simulations confirm the basic picture that the probability to initiate TA at each beat is determined by the
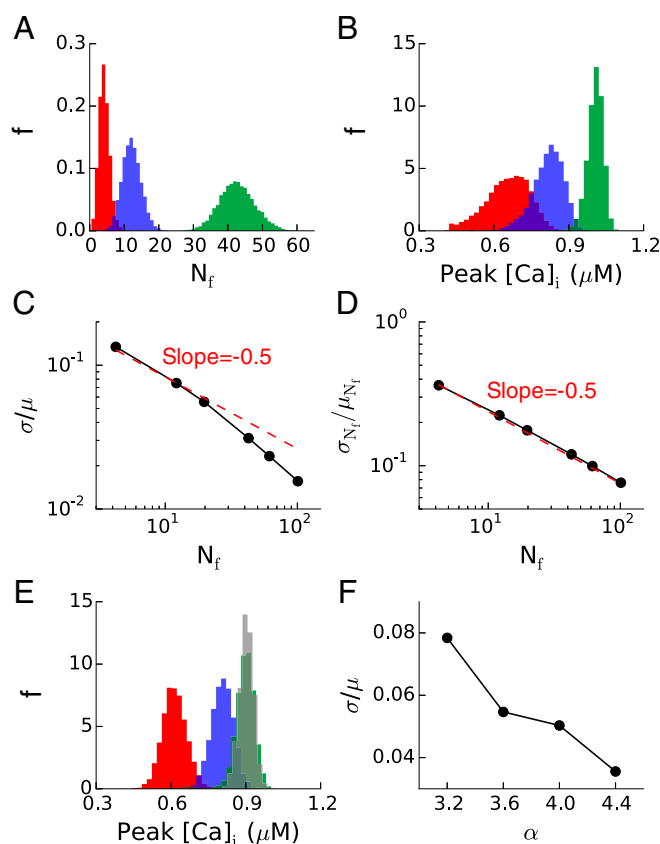

Fig. 4. Fluctuations in number of Ca^{2+} wave foci in lattice model of SCR. (*A*) Statistical distribution of the number of independent Ca^{2+} wave foci, N_f, for three different nucleation rates of wave foci: $k_f = 10^{-6}$ ms^{-1}·μm^{-3} (red), $k_f = 5 \times 10^{-6}$ ms^{-1}·μm^{-3} (blue), and $k_f = 30 \times 10^{-6}$ ms^{-1}·μm^{-3} (green). (*B*) Peak [Ca]$_i$ distributions corresponding to the cases in *A*. (*C*) Coefficient of variation (ratio of SD σ to mean μ) of peak [Ca]$_i$ vs. mean number of Ca^{2+} wave foci, which was increased by increasing k_f in the range from 10^{-6} to 10^{-4} ms^{-1}·μm^{-3} ($k_f = 10^{-6}$, 5×10^{-6}, 10×10^{-6}, 30×10^{-6}, 50×10^{-6}, and 10^{-4} ms^{-1}·μm^{-3}). The $-1/2$ slope in the log–log plot indicates that $\sigma/\mu \sim 1/\sqrt{<N_f>}$. (*D*) Coefficient of variation of the number of Ca^{2+} wave foci corresponding to the same k_f values in *C*. (*E*) Peak [Ca]$_i$ distribution in the detailed myocyte model for $\alpha = 3.2$ (red), $\alpha = 3.25$ (blue), $\alpha = 4$ (green), and $\alpha = 4.4$ (gray), PCL = 1 s. (*F*) Coefficient of variation of peak [Ca]$_i$ for the same α values in *E*.

summation of stochastic Ca^{2+} wave initiation events. Due to the randomness in the detailed myocyte model, the wave propagation distance may vary from site to site, as opposed to being cell wide as assumed in the lattice model. Despite its simplicity, the lattice model reproduces semiquantitatively well the increase of peak of the SCR amplitude distribution and narrowing of the width with increasing RyR hyperactivity. This is a direct consequence of the fact that N_f increases with hyperactivity and that the noise at the whole-cell level scales as $1/\sqrt{<N_f>}$. This scaling follows from the fact that each Ca^{2+} wave recruits CRUs over a finite volume of the cell $\sim$(total volume of the cell)/$<N_f>$ during a time window that is self-consistently determined to be the mean distance between wave foci divided by the wave propagation speed. Each region has a finite probability of being recruited at each beat, and consequently the SCR amplitude (peak whole-cell [Ca]$_i$), which is the summation of Ca^{2+} releases in each region, follows approximately a binomial distribution with a width $\sim\sqrt{<N_f>}$. Because the number of independent regions is smaller than the total number of CRUs ($N_f \ll N_{CRU}$), the relevant noise at the whole-cell level that determines the degree of randomness of TA ($\sim 1/\sqrt{<N_f>}$) is much larger than the noise level ($\sim 1/\sqrt{<N_{CRU}>}$) that would be expected if CRUs fired independently. For different model parameters, or in

experiments, N_f could be larger or smaller than in the present detailed model simulations but is expected to be always much smaller than N_{CRU}.

Bistability Between Bursting and Silent States Due to Positive Feedback Between SCR and Voltage Excitation. As shown in Fig. 1, as α is increased, the dynamics changes from subthreshold DADs, to transient TA bursts, and then to sustained voltage oscillations. Voltage oscillations become sustained when the probability of TA termination $(1 - p_{TAP})$, with p_{TAP} defined by Eq. **4**, becomes negligibly small. Whether transient or sustained, once a TAP is initiated, the burst length does not depend on the initial pacing history (Fig. 2F). This indicates that the TA burst behaves as a dynamical attractor of the system. Fig. 5A plots voltage against $[Ca]_i$ (log–log plot) for a TA burst, showing the exit from the limit cycle (black line) to the resting state (solid circle) via a subthreshold SCR (red line). Fig. 5B shows the N_{TAP} vs. α for PCL = 300 ms. When α is small ($\alpha \leq 2$), no TA occurs. As α is increased, TA occurs, and the burst lengths become longer with larger variations. When α is above another threshold ($\alpha \geq 3.3$), the TA burst becomes sustained. Therefore, the initiation and termination of TA are random transitions between two stable states: the excitable quiescent state (resting state) and the limit cycle oscillatory state. Underlying this bistable dynamics is a positive-feedback loop between AP excitation and SCR. Specifically, AP excitation has two effects. First, it brings in more Ca^{2+} via LCCs to increase the Ca^{2+} load and enhance CICR. Second, it causes the CRUs to fire synchronously so that they recover at roughly the same time. Both effects play important roles in promoting a subsequent SCR of a large amplitude that can then trigger an AP. Therefore, a positive-feedback loop forms between AP excitation and SCR.

To better demonstrate the positive feedback between voltage excitation and SCR in promoting bistability, we add a background Ca^{2+} leak current (*Methods*) to maintain a steady-state high Ca^{2+} load in the absence of pacing (pacing is needed to maintain a high Ca^{2+} load in the simulations above). We then carry out simulations by changing the conductance of this leak current to alter the Ca^{2+} load. Fig. 6A shows a simulation for a small Ca^{2+} leak current ($g_{Cab} = 9.3$ μS/μF). Before an AP is stimulated, the system is in a steady state with dyssynchronous SCRs, manifested as random spark clusters and miniwaves. During the stimulated AP, the CRUs fire synchronously due to the opening of the LCCs, resulting in a large whole-cell Ca^{2+} signal. After the AP, a synchronous SCR occurs to induce a DAD. The SR Ca^{2+} load is higher after the AP than before the AP (marked by the horizontal dashed line). After the DAD, the Ca^{2+} dynamics become dyssynchronous again with random spark clusters and miniwaves, and the SR Ca^{2+} load gradually decays to the same steady state before the AP. Therefore, the voltage excitation brings in more

Ca^{2+} and synchronizes CRUs, promoting a synchronous whole-cell SCR.

As the Ca^{2+} load is increased by increasing the leak conductance, the amplitude of the SCR becomes larger. Under this condition, a paced AP can then trigger a TA burst or sustained oscillations. Fig. 6B shows an example ($g_{Cab} = 14$ μS/μF) in which the TA is a sustained oscillation (see N_{TAP} vs. g_{Cab} in Fig. 6C). Before the stimulated AP, the Ca^{2+} release events are dyssynchronous, exhibiting random spark clusters and miniwaves. After a stimulated AP, a synchronous SCR results in a large enough amplitude to trigger another AP, and vice versa. Therefore, the positive-feedback loop between SCR and AP excitation maintains the repetitive firings of TA. To show the importance of the positive feedback, we block I_{Na} during one TAP (marked by the red bar in Fig. 6B) to break the feedback loop, the TA train stops and the Ca^{2+} release becomes dyssynchronous gradually, to the same steady state as before the stimulated AP.

The length of a TA burst depends on the level of Ca^{2+} load (Fig. 6C). When Ca^{2+} load is low (e.g., $g_{Cab} = 8.1$ μS/μF), no TA is observed. As Ca^{2+} load is increased, the number of TAPs in a burst of TA increases. When Ca^{2+} load is high enough (e.g., $g_{Cab} = 14$ μS/μF), TA is sustained for at least 50 beats (corresponding to the maximum length of the simulation) for all 100 trials. Fig. 6D shows that the N_{TAP} distribution for $g_{Cab} = 10.5$ and 11.6 μS/μF follow pure geometric distributions. To relate the bursting behavior to the intracellular Ca^{2+} dynamics, we measure the peak $[Ca]_i$ distribution for $g_{Cab} = 11.6$ μS/μF, which is shown in *SI Appendix*, Fig. S8. The distribution is truncated at $[Ca]_i \sim 1.15$ μM. To obtain the complete peak $[Ca]_i$ distribution, we block I_{Na} after the fifth TAP and record the next peak $[Ca]_i$. The resulting distributions for three g_{Cab} values are shown in Fig. 6E. Using the same fitting method as in Figs. 2 and 3, we fit the N_{TAP} distributions in Fig. 6D to Eq. **3** to obtain the p_{TAP} values. We then use the p_{TAP} values together with Gaussian fits of the distributions in Fig. 6E to determine Ca_{th} values, which are all close to 1.15 μM (*SI Appendix*, Table S4).

Discussion

Statistical Properties of Initiation and Termination of TA and SCR. We have shown that both the initiation of TA during pacing and the termination of a TA burst following cessation of pacing are highly random events. Randomness is reflected by the fact that both the number of DADs before initiation of a TA burst, which is characterized by coupled V_m and $[Ca]_i$ oscillations, and the number of oscillation cycles during a TA burst follows geometric distributions. Because DADs are caused by SCR events, we have characterized the statistical properties of those events to explain the randomness in initiation and termination of TA. By judicious manipulation of I_{Na} and $I_{Ca,L}$, we have been able to compute the full statistical distributions of the amplitude and timing of SCR events during pacing and TA bursts, accounting for both subthreshold and suprathreshold DADs. Access to the full distributions has been critically important to understand the origin of randomness.

The results reveal that SCR amplitude, as measured by the peak value of the whole-cell $[Ca]_i$, follows a broad normal distribution, whereas the distribution of spike waiting times after the last AP upstroke is comparatively much narrower. This difference can be attributed to the fact that the AP upstroke triggers nearly synchronized Ca^{2+} releases from CRUs, thereby causing SCR to occur at a relatively precise time interval after this upstroke when enough RyRs are recovered. Therefore, randomness of TA in cardiac myocyte is predominantly linked to spike amplitude but not timing. This is in contrast to other eukaryotic cells where Ca^{2+} dynamics is not coupled to V_m and randomness is manifested in both spike timing and amplitude (28, 37).

We have shown that the knowledge of the SCR amplitude normal distribution can be used to explain quantitatively the
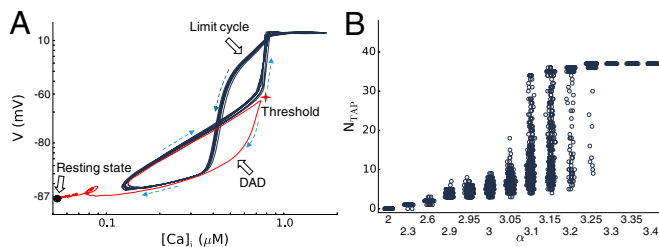
Fig. 5. Bistability in coupled voltage and intracellular Ca^{2+} dynamics. (A) Log–log plot of voltage vs. $[Ca]_i$ during a TA burst (black) and its termination via a subthreshold DAD (red), showing the transition between a limit cycle and the excitable resting state (black filled circle). Dashed arrows indicate the direction of the trajectory. The red star indicates the voltage and $[Ca]_i$ thresholds for TA. (B) The number of beats in a TA burst N_{TAP} vs. α where, for each α, at least 500 random trials are carried out; PCL = 0.3 s.

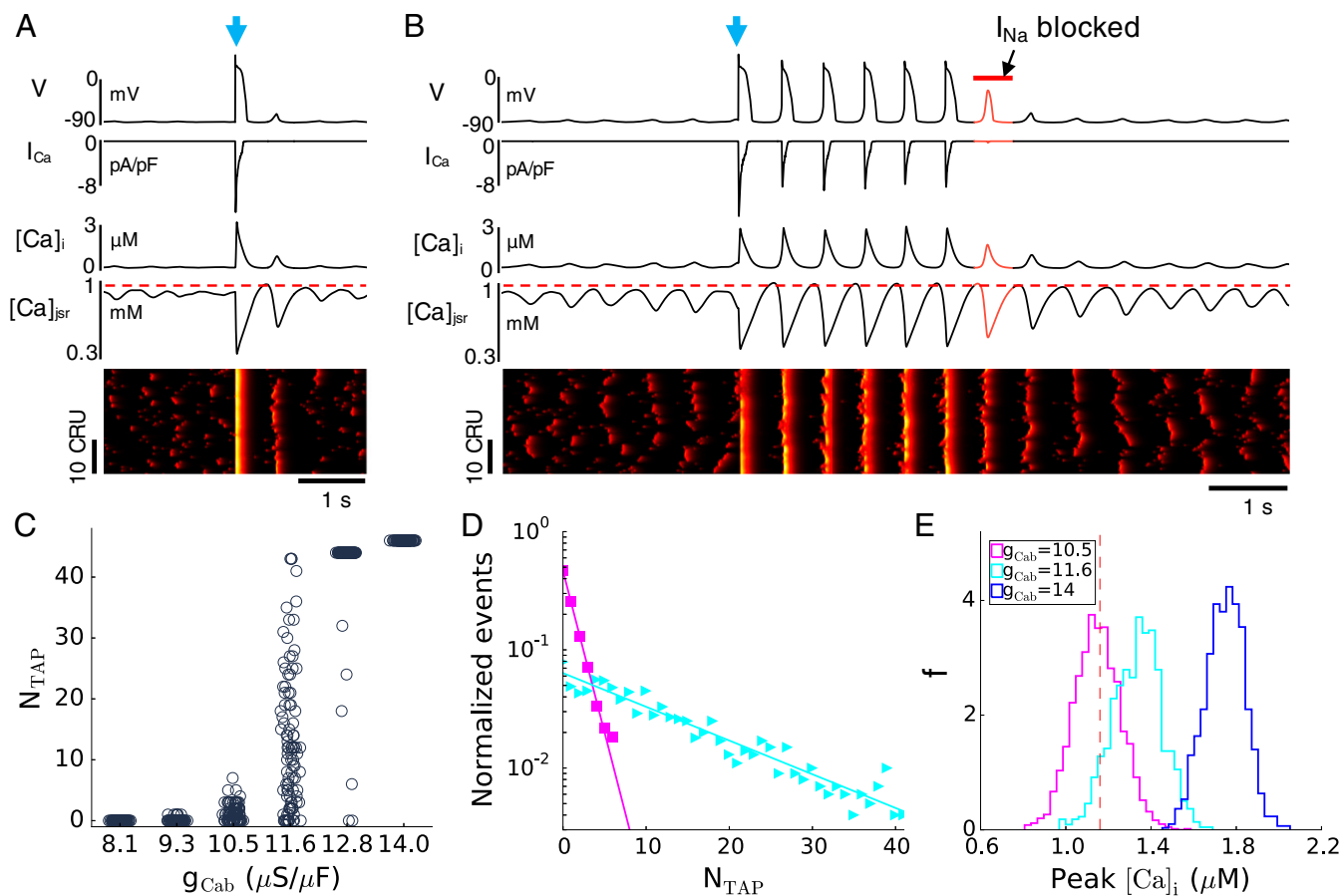**Fig. 6.** Positive feedback between SCR and AP excitation. A background Ca^{2+} current is incorporated into the model to maintain a stable steady-state high-Ca^{2+} load in the absence of pacing. The extracellular Ca^{2+} concentration $[Ca]_o$ is raised to 3 mM from 1.8 mM and $\alpha = 2$ without ISO stimulation. (*A*) A DAD following a paced beat (arrow) for $g_{Cab} = 9.3$ μS/μF. From *Top* to *Bottom*: V_m, $I_{Ca,L}$, $[Ca]_i$, and $[Ca]_{jsr}$ vs. time, and a line-scan image of cytosolic Ca^{2+} concentration. (*B*) TA burst following a paced beat (arrow) for $g_{Cab} = 14$ μS/μF, which is terminated by blocking I_{Na} in the time window as indicated by the red bar. The layout is the same as *A*. (*C*) Number of TAPs during a TA burst vs. g_{Cab}. At least 100 independent random trials are carried out for each g_{Cab}. (*D*) N_{TAP} distribution for $g_{Cab} = 10.5$ (magenta) and 11.6 (cyan) μS/μF. Lines are best fits to Eq. **3** with R^2 being 0.999 (magenta line) and 0.914 (cyan line). (*E*) Peak $[Ca]_i$ distributions obtained at the sixth SCR during which I_{Na} is blocked for $g_{Cab} = 10.5$ (magenta), 11.6 (cyan), and 14 (blue) μS/μF for at least 1,000 random trials. The dashed line in *E* marks the $[Ca]_i$ threshold for TA termination.

observed distributions of the number of DADs (N_{DAD}) before initiation of a TA burst and the number of TAPs (N_{TAP}) following a TA burst. It should be emphasized that this distribution is generally only quantitatively predictive of the initiation or termination of TA for values of N_{DAD} or N_{TAP} that exceed the number of beats required for the SCR amplitude distribution to relax to a stationary distribution. During a period varying from one to a few beats depending on the protocol used to induce TA, the total Ca^{2+} inside the cell adjusts to a new level as a result of the balance between Ca^{2+} entry via LCCs and extrusion via the forward mode of NCX. For the protocol where TA is induced by RyR hyperactivity and ISO stimulation, this relaxation process is illustrated in *SI Appendix*, Fig. S9, which shows that it takes several beats for $[Ca]_i$ and $[Ca]_{SR}$ to reach new steady-state cycles (peaks and nadirs) after the transition from pacing to spontaneous TA. Because the peak $[Ca]_i$ is higher during the transient period than in the steady state, it is less likely that a fluctuation brings $[Ca]_i$ below the threshold for termination of TA. As a result, the probability of termination is lower than expected from the steady-state geometric distribution for small N_{TAP}, as seen in Fig. 2*E* where the distribution becomes purely geometric for $N_{TAP} > 6$. For the case where TA is induced by the combination of increasing the extracellular Ca^{2+} concentration and adding a background Ca^{2+} current, Fig. 6*B* shows that both $[Ca]_i$ and $[Ca]_{SR}$ relax quickly to new steady

states and the N_{TAP} distributions (Fig. 6*D*) are purely geometric for all N_{TAP} values.

The SCR amplitude threshold for initiation or maintenance of TA is governed predominantly by I_{NCX} that promotes membrane depolarization. Hence, physiological conditions that affect I_{NCX}, such as the extracellular Ca^{2+} concentration $[Ca]_o$, influence this threshold. This is illustrated in *SI Appendix*, Fig. S6, which shows that a larger peak $[Ca]_i$ is required to drive the same amplitude I_{NCX} when $[Ca]_o$ is increased. As a result, the SCR amplitude threshold for TA is significantly larger in Fig. 6*E* with elevated $[Ca]_o$ ($Ca_{th} \sim 1.15$ μM) than Fig. 3*E* ($Ca_{th} \sim 0.75$ μM) with normal $[Ca]_o$. More generally, this threshold could also be influenced by I_{K1}, which is the dominant repolarizing current for the range of membrane potential near the resting state. A subtler effect is that the threshold for initiation and termination of TA can differ slightly under the same conditions ($Ca_{th} \sim 0.69$ μM for initiation vs. $Ca_{th} \sim 0.75$ μM for termination in Fig. 3*E*). This small difference can be attributed to the fact that peak $[Ca]_i$ is only a "global" measure of a SCR event integrated over space and time. As a result, different events with different spatiotemporal patterns of Ca^{2+} release may produce the same peak $[Ca]_i$, but yield slightly different peak I_{NCX} and DAD amplitudes. This interpretation is supported by the observation that the truncated SCR amplitude distributions in Fig. 3 *B* and *E* do not terminate abruptly, but are

smeared over a narrow range of $[Ca]_i$ near Ca_{th}. Despite this limitation, our results in Figs. 3 and 6 show that peak $[Ca]_i$, which is an experimentally observable property, provides a good quantitative measure of the propensity of a SCR event to stochastically initiate or terminate TA under different conditions.

Ion Channel Stochasticity vs. Whole-Cell–Level Randomness. During normal activity, both the AP and the Ca^{2+} transient are highly reproducible despite a high level of ion channel stochasticity. It is well understood that, except in special cases (6, 50–52), the noise in the voltage signal is averaged out at the whole-cell level by the fact that there is a very large number of voltage-gated ion channels of any given type and that voltage is spatially uniform on the scale of a myocyte. Similarly, the noise in the Ca^{2+} signal in turn is averaged out by the fact that, during normal excitation–contraction coupling, CICR mediated by LCC openings is relatively synchronous, with a very large number of CRUs participating in the whole-cell Ca^{2+} release. It is well appreciated that, in contrast, SCR can have a more random character. However, the origin of this randomness in cardiac myocytes has remained unclear.

In the well-studied case where Ca^{2+} cycling dynamics is not coupled to V_m (28, 37), SCR events (also referred to as Ca^{2+} puffs) have a relatively low rate of occurrence. As a result, intervals between events follow an exponential waiting-time distribution characteristic of an inhomogeneous Poisson process. In the setting of cardiac myocytes, our results show that the timing of SCR is relatively precise, but amplitudes are much more random. As already explained, the narrow distribution of timing is due to the fact that RyR channels become available for release after a fixed recovery time following an excitation that produces synchronized Ca^{2+} releases. In this setting, a broad normal distribution of SCR amplitude follows then naturally from the additional property that the rate of initiation of Ca^{2+} waves is relatively high after RyR channels are recovered. As a result, several wave foci can form and jointly contribute to a single whole-cell SCR event and DAD. Because wave foci form independently and the SCR amplitude is a summation of waves (i.e., of unitary Ca^{2+} releases of CRUs recruited by each wave), the coefficient of variation of SCR amplitude scales approximately as $1/\sqrt{<N_f>}$, where $<N_f>$ is the average number of wave foci. This number can vary from about 5 to 50 in simulations and experiments depending on the properties of RyR channels and Ca^{2+} load. In all cases, this number is much smaller than the number of CRUs, thereby causing large fluctuation in SCR amplitude at the whole-cell level that in turn causes the initiation and termination of TA to appear random.

It is possible that, under certain conditions (e.g., less pronounced RyR leakiness), the rate of initiation of Ca^{2+} waves could be relatively low after RyR channels are recovered. In such a case, one would expect a whole-cell SCR event to be triggered by the propagation of a single Ca^{2+} wave and the distribution of waiting times after excitation to be exponential. Such a condition could potentially initiate a single DAD and TAP after cessation of pacing but would be unlikely to initiate TA during pacing or to maintain sustained bursts of TA. We therefore expect the situation in which several Ca^{2+} waves contribute to SCR to underlie the commonly observed forms of TA relevant for arrhythmias.

Positive Feedback Between Voltage Excitation and SCR. We have shown in this study that the positive feedback between AP excitation and SCR is key to maintaining a TA burst. In general, increased RyR channel leakiness and Ca^{2+} load promoted by rapid pacing cause the peak of the SCR amplitude distribution to shift toward higher $[Ca]_i$, causing more frequent SCR events that can trigger APs. Under normal coupling conditions, no SCR events occur, and Ca^{2+} release is triggered by LCC openings during AP excitation. As Ca^{2+} load and RyR open probability are increased, SCR can occur due to CICR in the Ca^{2+} cycling system. AP excitation enhances CICR by bringing Ca^{2+} into the cell and

synchronizing the firing of CRUs. When the SCR amplitude is below the threshold for TA, SCR only leads to DADs. As Ca^{2+} load and RyR open probability are increased further, the amplitude of SCR increases above the threshold for TA initiation. Once TA occurs, a positive-feedback loop forms in which SCR triggers an AP, AP activation then potentiates a new SCR by increasing Ca^{2+} load and CRU synchronization, and this subsequent SCR in turn triggers an AP.

This positive-feedback loop underlies a new limit cycle attractor, resulting in bistability between this limit cycle and the silent resting state. Because the RyRs open randomly, the number of foci of Ca^{2+} waves is random, causing random SCR amplitudes. This randomness causes random switches between the two attractors, resulting in TA bursts. After escape from the metastable limit cycle, V_m returns to the stable resting state followed by a paced train of normal APs of variable duration until TA is again initiated. This can lead to complex forms of parasystole in which trains of paced APs are interspersed with bursts of TA. Furthermore, for TA to be initiated during pacing, the PCL must be sufficiently long for SCR to occur during diastole. For shorter PCL, initiation of TA requires a pause after pacing for SCR to occur. Hence, initiation of TA generally depends on both pacing history and statistical properties of SCR. For intermediate levels of RyR leakiness, the lifetime of TA bursts will be highly variable because N_{TAP} follows in this case a broad geometric distribution. As SCR is strengthened further, the probability of TA termination becomes vanishingly small (i.e., DADs are always suprathreshold) and the limit cycle becomes essentially stable.

Limitations. Some limitations of the present study are worth pointing out. The CRU network is assumed to be regular while heterogeneities in the number of RyRs in each CRU and CRU spacing (34, 53), which are present in real myocytes, may affect intracellular Ca^{2+} dynamics. We use a model of RyR kinetics that incorporates a luminal gate and RyR refractoriness based on experimental observations (43, 44). However, it has been shown that RyR refractoriness is not required for spark termination during normal Ca^{2+} transients (54–57), and whether RyRs exhibit refractoriness in cardiac myocytes is still in debate (58, 59). We test the effect of eliminating RyR refractoriness (*SI Appendix*, section J and Fig. S10). We find that it does not prevent spark termination, consistent with other modeling studies (54, 55), but suppresses DADs because increased RyR leakiness reduces the SR load below the threshold for Ca^{2+} wave initiation. This result suggests that RyR refractoriness may be required for TA. Finally, our model assumes that the Ca^{2+} concentration is spatially uniform inside the submicron dyadic space. Higher-resolution models (56, 60, 61) can relax this assumption
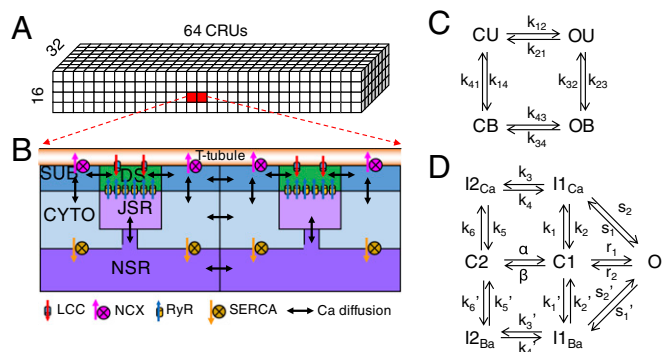

Fig. 7. Schematics of the ventricular myocyte model. (*A*) Schematic plot of the ventricular myocyte model consisting of $64 \times 32 \times 16$ CRUs. (*B*) The coupling between different compartments and CRUs. CYTO, cytosolic space; DS, dyadic space; JSR, junctional SR; NSR, network SR; SUB, submembrane space. (*C*) The four-state RyR model. (*D*) The Markov LCC model.

but remain computationally prohibitive to characterize statistical properties of TA.

Conclusions and Outlook

In summary, our results demonstrate that a stochastic bistable switch between the resting silent state and a limit cycle consisting of bidirectionally coupled voltage and Ca^{2+} oscillations is the underlying mechanism of TA in cardiac myocytes. Bistability originates from a positive feedback between voltage excitation and SCR. Randomness in turn originates from fluctuations in the number of Ca^{2+} wave foci that underlies a broad normal distribution of SCR amplitude. Because DAD-mediated TA is a candidate mechanism of PVCs in ventricular arrhythmias, our study provides important insights into different PVC patterns (4) or nonsustained episodes of ventricular tachycardia (3). Importantly, the mechanism of TA burst can be a candidate mechanism for nonsustained ventricular tachycardia. This assumes that similar mechanisms elucidated here for isolated cardiac myocytes extend to a tissue scale, which sometimes may not be straightforward (62). Owing to the property that the distribution of waiting times of SCR events following excitation is narrow, we expect DADs to occur synchronously in a large enough number of cells to initiate TA when cells are electrically coupled. However, heterogeneity of cellular properties could further complexify the mechanisms of initiation and termination by introducing another source of randomness that is distinct from ion channel stochasticity. Extending the present investigation to the tissue scale is made extremely challenging by the fact that simulations that resolve the stochastic and spatially distributed nature of Ca^{2+} release are only presently feasible for small networks of cells. However, the statistical properties of intracellular Ca^{2+} dynamics and initiation and termination of TA elucidated here should already be experimentally testable in isolated myocyte experiments. Finally, the present insights into the positive feedback between voltage and Ca^{2+} dynamics may also be relevant for understanding the coupling of the voltage and Ca^{2+} "clocks" in the related setting of sinoatrial node pacemaking cells (63–65).

Methods

The mathematical formulations and parameters of the ventricular myocyte model were presented in detail in a recent study by Song et al. (39). Here, we outline the model briefly.

The spatiotemporal Ca^{2+} cycling model is based on the one developed by Restrepo et al. (43, 44), which consists of a 3D network of $64 \times 32 \times 16$ CRUs (Fig. 7A). Each CRU includes the following subvolumes (Fig. 7B): a cytosolic space (CYTO), a submembrane space (SUB), a dyadic space (DS), a junctional SR (JSR), and a network SR (NSR). These subvolumes are linked either by Ca^{2+} diffusion or by SR Ca^{2+} release or uptake. The CRUs are coupled to the extracellular space via LCCs and NCX. Neighboring CRUs are coupled via Ca^{2+} diffusion in the cytosol and SR.

The membrane ionic current formulations are from the rabbit ventricular myocyte model (39, 45), with the membrane potential (V_m) described by the following:

$$C_m \frac{dV_m}{dt} = -(I_{Na} + I_{Ca,L} + I_{Ks} + I_{Kr} + I_{NCX} + I_{NaK} + I_{K1} + I_{to,f} + I_{to,s} + I_{Cab} + I_{sti}),\quad [5]$$

where $C_m = 1\ \mu F/cm^2$ is the membrane capacitance and I_{sti} is the stimulus current density. $I_{Ca,L}$ is a summation of the unitary currents of the CRUs, that is, $I_{Ca,L} = \sum_{k=1}^{N \times m} i_{LCC}(k)$, where N is the total number of CRUs and m is the total number of LCCs in a CRU. We choose $m = 4$ for control. I_{NCX} is also a summation of the unitary current of the CRUs, that is, $I_{NCX} = \sum_{k=1}^{N} i_{NCX}(k)$. We add a leak Ca^{2+} current (I_{Cab}), which is described by $I_{Cab} = g_{Cab}(V - E_{Ca})$, where $E_{Ca} = (RT/2F)\ln([Ca]_o/[Ca]_i)$ is the reverse potential. Varying the conductance of I_{Cab} changes the diastolic Ca^{2+} concentration in the cytosol and SR. For simulations in Figs. 1–5, $g_{Cab} = 0$. For simulations in Fig. 6, g_{Cab} values vary from 8 to 14 $\mu S/\mu F$.

The gating kinetics of RyR is described by a Markov model (Fig. 7C), which is simulated stochastically. To simulate hyperactive RyRs, we introduce a multiplicative factor α into the RyR gating kinetics:

$$k_{12} = \alpha K_u c_p^2 \text{ and } k_{43} = \alpha K_b c_p^2,\quad [6]$$

where c_p is the Ca^{2+} concentration in the dyadic space, and K_u and K_b are the rate constants used in the original model ($K_u = 0.00038\ \mu M^{-2} \cdot ms^{-1}$ and $K_b = 0.00005\ \mu M^{-2} \cdot ms^{-1}$). Increasing α increases the RyR open probability.

The gating kinetics of LCCs is also described by a Markov model (Fig. 7D) and simulated stochastically. To simulate β-adrenergic stimulation, we modify the SERCA and the LCC properties. Specifically, we double both the SERCA pump strength and the number of LCCs in a CRU. We also reduce s_1 and s_1' by 50%, and increase r_1 to three times its original value. s_1, s_1', and r_1 are transition rates of the original LCC model and are denoted in Fig. 7D.

The integration of differential equations is performed using the Euler method. The time step for integration is 0.1 ms.

1. Zipes DP, Wellens HJ (1998) Sudden cardiac death. *Circulation* 98(21):2334–2351.
2. Zipes DP, Rubart M (2006) Neural modulation of cardiac arrhythmias and sudden cardiac death. *Heart Rhythm* 3(1):108–113.
3. Glass L (2005) Multistable spatiotemporal patterns of cardiac activity. *Proc Natl Acad Sci USA* 102(30):10409–10410.
4. Qu Z, Hu G, Garfinkel A, Weiss JN (2014) Nonlinear and stochastic dynamics in the heart. *Phys Rep* 543(2):61–162.
5. Sato D, et al. (2009) Synchronization of chaotic early afterdepolarizations in the genesis of cardiac arrhythmias. *Proc Natl Acad Sci USA* 106(9):2983–2988.
6. Lerma C, Krogh-Madsen T, Guevara M, Glass L (2007) Stochastic aspects of cardiac arrhythmias. *J Stat Phys* 128(1–2):347–374.
7. Lemay M, de Lange E, Kucera JP (2011) Effects of stochastic channel gating and distribution on the cardiac action potential. *J Theor Biol* 281(1):84–96.
8. Pogwizd SM, Bers DM (2002) Calcium cycling in heart failure: The arrhythmia connection. *J Cardiovasc Electrophysiol* 13(1):88–91.
9. Hoeker GS, Katra RP, Wilson LD, Plummer BN, Laurita KR (2009) Spontaneous calcium release in tissue from the failing canine heart. *Am J Physiol Heart Circ Physiol* 297(4): H1235–H1242.
10. Ross JL, Howlett SE (2009) β-Adrenoceptor stimulation exacerbates detrimental effects of ischemia and reperfusion in isolated guinea pig ventricular myocytes. *Eur J Pharmacol* 602(2-3):364–372.
11. Watanabe H, et al. (2009) Flecainide prevents catecholaminergic polymorphic ventricular tachycardia in mice and humans. *Nat Med* 15(4):380–383.
12. Liu N, et al. (2013) Abnormal propagation of calcium waves and ultrastructural remodeling in recessive catecholaminergic polymorphic ventricular tachycardia. *Circ Res* 113(2):142–152.
13. Bai Y, et al. (2013) Phospholamban knockout breaks arrhythmogenic Ca^{2+} waves and suppresses catecholaminergic polymorphic ventricular tachycardia in mice. *Circ Res* 113(5):517–526.
14. Lou Q, et al. (2015) Alternating membrane potential/calcium interplay underlies repetitive focal activity in a genetic model of calcium-dependent atrial arrhythmias. *J Physiol* 593(6):1443–1458.
15. Shiferaw Y, Aistrup GL, Wasserstrom JA (2012) Intracellular Ca^{2+} waves, afterdepolarizations, and triggered arrhythmias. *Cardiovasc Res* 95(3):265–268.
16. Ter Keurs HEDJ, Boyden PA (2007) Calcium and arrhythmogenesis. *Physiol Rev* 87(2):457–506.
17. Pogwizd SM, Bers DM (2004) Cellular basis of triggered arrhythmias in heart failure. *Trends Cardiovasc Med* 14(2):61–66.
18. Kashimura T, et al. (2010) In the RyR2(R4496C) mouse model of CPVT, β-adrenergic stimulation induces SR Ca waves by increasing SR Ca content and not by decreasing the threshold for Ca waves. *Circ Res* 107(12):1483–1489.
19. Venetucci LA, Trafford AW, Eisner DA (2007) Increasing ryanodine receptor open probability alone does not produce arrhythmogenic calcium waves: Threshold sarcoplasmic reticulum calcium content is required. *Circ Res* 100(1):105–111.
20. Johnson N, Danilo P, Jr, Wit AL, Rosen MR (1986) Characteristics of initiation and termination of catecholamine-induced triggered activity in atrial fibers of the coronary sinus. *Circulation* 74(5):1168–1179.
21. Wasserstrom JA, et al. (2010) Variability in timing of spontaneous calcium release in the intact rat heart is determined by the time course of sarcoplasmic reticulum calcium load. *Circ Res* 107(5):1117–1126.
22. Fujiwara K, Tanaka H, Mani H, Nakagami T, Takamatsu T (2008) Burst emergence of intracellular Ca^{2+} waves evokes arrhythmogenic oscillatory depolarization via the Na^+-Ca^{2+} exchanger: Simultaneous confocal recording of membrane potential and intracellular Ca^{2+} in the heart. *Circ Res* 103(5):509–518.
23. Brunello L, et al. (2013) Decreased RyR2 refractoriness determines myocardial synchronization of aberrant Ca^{2+} release in a genetic model of arrhythmia. *Proc Natl Acad Sci USA* 110(25):10312–10317.
24. Xing D, Martins JB (2004) Triggered activity due to delayed afterdepolarizations in sites of focal origin of ischemic ventricular tachycardia. *Am J Physiol Heart Circ Physiol* 287(5):H2078–H2084.

25. Sedej S, et al. (2010) Na$^+$-dependent SR Ca^{2+} overload induces arrhythmogenic events in mouse cardiomyocytes with a human CPVT mutation. *Cardiovasc Res* 87(1):50–59.

26. Falcke M (2003) On the role of stochastic channel behavior in intracellular Ca^{2+} dynamics. *Biophys J* 84(1):42–56.

27. Nivala M, Ko CY, Nivala M, Weiss JN, Qu Z (2012) Criticality in intracellular calcium signaling in cardiac myocytes. *Biophys J* 102(11):2433–2442.

28. Skupin A, et al. (2008) How does intracellular Ca^{2+} oscillate: By chance or by the clock? *Biophys J* 94(6):2404–2411.

29. Skupin A, Kettenmann H, Falcke M (2010) Calcium signals driven by single channel noise. *PLoS Comput Biol* 6(8):e1000870.

30. Chan Y-H, et al. (2015) Acute reversal of phospholamban inhibition facilitates the rhythmic whole-cell propagating calcium waves in isolated ventricular myocytes. *J Mol Cell Cardiol* 80:126–135.

31. Wang K, Rappel WJ, Levine H (2004) Cooperativity can reduce stochasticity in intracellular calcium dynamics. *Phys Biol* 1(1-2):27–34.

32. Chen W, Aistrup G, Wasserstrom JA, Shiferaw Y (2011) A mathematical model of spontaneous calcium release in cardiac myocytes. *Am J Physiol Heart Circ Physiol* 300(5):H1794–H1805.

33. Nivala M, Ko CY, Nivala M, Weiss JN, Qu Z (2013) The emergence of subcellular pacemaker sites for calcium waves and oscillations. *J Physiol* 591(21):5305–5320.

34. Soeller C, Crossman D, Gilbert R, Cannell MB (2007) Analysis of ryanodine receptor clusters in rat and human cardiac myocytes. *Proc Natl Acad Sci USA* 104(38):14958–14963.

35. Chen-Izu Y, et al. (2007) Phosphorylation of RyR2 and shortening of RyR2 cluster spacing in spontaneously hypertensive rat with heart failure. *Am J Physiol Heart Circ Physiol* 293(4):H2409–H2417.

36. Franzini-Armstrong C, Protasi F, Ramesh V (1999) Shape, size, and distribution of Ca^{2+} release units and couplons in skeletal and cardiac muscles. *Biophys J* 77(3):1528–1539.

37. Skupin A, Falcke M (2009) From puffs to global Ca^{2+} signals: How molecular properties shape global signals. *Chaos* 19(3):037111.

38. Karma A (2013) Physics of cardiac arrhythmogenesis. *Annu Rev Condens Matter Phys* 4(1):313–337.

39. Song Z, Ko CY, Nivala M, Weiss JN, Qu Z (2015) Calcium-voltage coupling in the genesis of early and delayed afterdepolarizations in cardiac myocytes. *Biophys J* 108(8):1908–1921.

40. Shiferaw Y, Karma A (2006) Turing instability mediated by voltage and calcium diffusion in paced cardiac cells. *Proc Natl Acad Sci USA* 103(15):5670–5675.

41. Gaeta SA, Bub G, Abbott GW, Christini DJ (2009) Dynamical mechanism for subcellular alternans in cardiac myocytes. *Circ Res* 105(4):335–342.

42. Krogh-Madsen T, Christini DJ (2012) Nonlinear dynamics in cardiology. *Annu Rev Biomed Eng* 14:179–203.

43. Restrepo JG, Weiss JN, Karma A (2008) Calsequestrin-mediated mechanism for cellular calcium transient alternans. *Biophys J* 95(8):3767–3789.

44. Restrepo JG, Karma A (2009) Spatiotemporal intracellular calcium dynamics during cardiac alternans. *Chaos* 19(3):037115.

45. Mahajan A, et al. (2008) A rabbit ventricular action potential model replicating cardiac dynamics at rapid heart rates. *Biophys J* 94(2):392–410.

46. El-Jouni W, Jang B, Haun S, Machaca K (2005) Calcium signaling differentiation during *Xenopus* oocyte maturation. *Dev Biol* 288(2):514–525.

47. Marchant J, Callamaras N, Parker I (1999) Initiation of IP$_3$-mediated Ca^{2+} waves in *Xenopus* oocytes. *EMBO J* 18(19):5285–5299.

48. Fontanilla RA, Nuccitelli R (1998) Characterization of the sperm-induced calcium wave in *Xenopus* eggs using confocal microscopy. *Biophys J* 75(4):2079–2087.

49. Wagner J, Li YX, Pearson J, Keizer J (1998) Simulation of the fertilization Ca^{2+} wave in *Xenopus laevis* eggs. *Biophys J* 75(4):2088–2097.

50. Tanskanen AJ, Greenstein JL, O'Rourke B, Winslow RL (2005) The role of stochastic and modal gating of cardiac L-type Ca^{2+} channels on early after-depolarizations. *Biophys J* 88(1):85–95.

51. Sato D, Xie LH, Nguyen TP, Weiss JN, Qu Z (2010) Irregularly appearing early after-depolarizations in cardiac myocytes: Random fluctuations or dynamical chaos? *Biophys J* 99(3):765–773.

52. Keener JP, Newby JM (2011) Perturbation analysis of spontaneous action potential initiation by stochastic ion channels. *Phys Rev E Stat Nonlin Soft Matter Phys* 84(1 Pt 1):011918.

53. Baddeley D, et al. (2009) Optical single-channel resolution imaging of the ryanodine receptor distribution in rat cardiac myocytes. *Proc Natl Acad Sci USA* 106(52):22275–22280.

54. Vierheller J, Neubert W, Falcke M, Gilbert SH, Chamakuri N (2015) A multiscale computational model of spatially resolved calcium cycling in cardiac myocytes: From detailed cleft dynamics to the whole cell concentration profiles. *Front Physiol* 6:255.

55. Sobie EA, Dilly KW, dos Santos Cruz J, Lederer WJ, Jafri MS (2002) Termination of cardiac Ca^{2+} sparks: An investigative mathematical model of calcium-induced calcium release. *Biophys J* 83(1):59–78.

56. Walker MA, et al. (2014) Superresolution modeling of calcium release in the heart. *Biophys J* 107(12):3018–3029.

57. Song Z, Karma A, Weiss JN, Qu Z (2016) Long-lasting sparks: Multi-metastability and release competition in the calcium release unit network. *PLoS Comput Biol* 12(1):e1004671.

58. Ramay HR, Liu OZ, Sobie EA (2011) Recovery of cardiac calcium release is controlled by sarcoplasmic reticulum refilling and ryanodine receptor sensitivity. *Cardiovasc Res* 91(4):598–605.

59. Belevych AE, et al. (2012) Shortened Ca^{2+} signaling refractoriness underlies cellular arrhythmogenesis in a postinfarction model of sudden cardiac death. *Circ Res* 110(4):569–577.

60. Weinberg SH, Smith GD (2014) The influence of Ca^{2+} buffers on free [Ca^{2+}] fluctuations and the effective volume of Ca^{2+} microdomains. *Biophys J* 106(12):2693–2709.

61. Wieder N, Fink R, von Wegner F (2015) Exact stochastic simulation of a calcium microdomain reveals the impact of Ca^{2+} fluctuations on IP$_3$R gating. *Biophys J* 108(3):557–567.

62. Qu Z, Weiss JN (2015) Mechanisms of ventricular arrhythmias: From molecular fluctuations to electrical turbulence. *Annu Rev Physiol* 77(1):29–55.

63. Lakatta EG (2010) A paradigm shift for the heart's pacemaker. *Heart Rhythm* 7(4):559–564.

64. Lakatta EG, Maltsev VA, Vinogradova TM (2010) A coupled SYSTEM of intracellular Ca^{2+} clocks and surface membrane voltage clocks controls the timekeeping mechanism of the heart's pacemaker. *Circ Res* 106(4):659–673.

65. Joung B, Ogawa M, Lin S-F, Chen P-S (2009) The calcium and voltage clocks in sinoatrial node automaticity. *Korean Circ J* 39(6):217–222.